Palaeogeography, Palaeoclimatology, Palaeoecology 562 (2021) 110090

Contents lists available at ScienceDirect

Palaeogeography, Palaeoclimatology, Palaeoecology

journal homepage: www.elsevier.com/locate/palaeo

# Nearshore paleoceanogaphic conditions through the Holocene: Shell carbonate from archaeological sites of the Atacama Desert coast

Carola Flores [a,*], Bernardo R. Broitman [b]

[a] Centro de Estudios Avanzados en Zonas Áridas (CEAZA), Facultad de Ciencias del Mar, Universidad Católica del Norte, Ossandón 877, Coquimbo, Chile
[b] Departamento de Ciencias, Facultad de Artes Liberales & Bioengineering Innovation Center, Facultad de Ingeniería y Ciencias, Universidad Adolfo Ibáñez, Viña del Mar, Chile

ARTICLE INFO

*Keywords:*
*Fissurella maxima* shell
Isotopic analysis
$\delta^{18}O$ $\delta^{13}C$
Coastal upwelling
Shell carbonate
Sea surface temperature

ABSTRACT

From the southern coast of Peru to the central-north coast of Chile (18°-31°S) previous evidence suggests that wide variations in sea surface temperature (SST) over the Holocene may be associated with changes in coastal upwelling regimes along the region. Support for spatial contrasts and similarities in oceanographic dynamics comes from earlier work at both extremes of the region. Using a 12 kyr record derived from shell midden archaeological sites around Taltal Chile (25°S), we show that changes in the region are not necessarily consistent with a simple latitudinal gradient. Using $\delta^{13}C$ and $\delta^{18}O$ isotopic records from archaeological carbonate shells of the keyhole limpet *Fissurella maxima* we find that cold SST during the Early Holocene was associated with more negative $\delta^{13}C$ values in agreement with observations from southern Peru. Warmer waters during the beginning of the Middle Holocene, had positive $\delta^{13}C$ values, differentiating them from southern Peru and central-north Chile records. The rest of the Middle Holocene showed a decreasing SST accompanied by negative $\delta^{13}C$ values, and after 4000 cal yr BP, the Late Holocene showed a progressive increase in SST and positive $\delta^{13}C$ values. Finally, modern carbonate shells of *F. maxima* indicate a situation not observed throughout the Holocene period: warm SST is associated with negative $\delta^{13}C$ values, in line with results on modern shells from southern Peru and modern oceanographic patterns that indicate an intensification of coastal upwelling with events of warm water intrusion. Our results show that the southern coast of the Atacama Desert experienced important fluctuations in SST and upwelling conditions during the Holocene, which may have affected the distribution of nearshore fisheries along the Northern Coast of Chile.

## 1. Introduction

There is widespread evidence of large global climatic variability during the Holocene and its impacts on human populations (Mayewski et al., 2004). Archaeological evidence shows a wide range of strategies developed by human societies under favorable and unfavorable climatic conditions such as migration, increased organization complexity and technological change (Anderson et al., 2007). In the case of coastal societies, climate variability linked to sea surface temperature (SST) anomalies like El Niño Southern Oscillation (ENSO) are well known to bring important consequences for people from the Holocene to the present (Caviedes, 2002; Richardson and Sandweiss, 2008). Therefore, broadening our understanding of the multiple climatic scenarios that unraveled during the Holocene is key to inform future human adaptation strategies (Zhang et al., 2011; McMichael, 2012).

Nearshore temperature patterns provide a linkage between coastal ecosystems and the oceanographic processes that regulate the fluxes of biotic and abiotic resources to shore (Menge et al., 2003; Navarrete et al., 2005). Therefore, SST variability is key to understanding climatic effects on nearshore ecosystems and its inhabitants. Along the temperate sectors of ocean's eastern boundaries, a key source of SST variability is wind-driven coastal upwelling. Cold, low oxygen and nutrient-rich deeper waters flowing poleward from the subtropics are transported upward through the combined effect of alongshore equatorward transport of surface waters by wind and their offshore displacement by the Coriolis Effect (Strub et al., 1998; Chavez and Messié, 2009).

In the present, the coast of southern Peru and northern Chile (18° to 30–31°S), is characterized by year-round upwelling-favorable conditions, which maintains one of the most productive pelagic fisheries worldwide (Strub et al., 1998; Montecino and Lange, 2009). While the

* Corresponding author.
*E-mail address:* carola.flores@ceaza.cl (C. Flores).

https://doi.org/10.1016/j.palaeo.2020.110090
Received 27 March 2020; Received in revised form 12 October 2020; Accepted 12 October 2020
Available online 15 October 2020

northern and central sector of this region exhibit high primary productivity over the narrow continental shelf, the southernmost sector experiences more intense and semi-permanent upwelling-favorable wind. South of 30–31°S upwelling-favorable wind conditions become more seasonal, peaking during early spring around 30–31° to late summer around of 36–37°S.This forcing pattern drives the formation of mesoscale eddies and filaments that transport recently upwelled waters and coastal productivity off the coastal transition zone (Hormazabal et al., 2004; Aguilera et al., 2019). Reconstructions of SST patterns and upwelling intensity from multiple lines of evidence, indicate that southern Peru and northern Chile (15°- 25°S) during the Early Holocene (11000–9000) experienced cooler conditions and higher upwelling intensity than present, while the central-north sector (31°S) experienced conditions similar to modern times (Carré et al., 2012, 2014, 2016; Flores et al., 2018; Ortlieb et al., 2011; Vargas et al., 2006,; Salvatteci et al., 2019a). Spatial variation in upwelling intensity between the Early Holocene and present time along the temperate coast off western South America suggests a persistent latitudinal difference in SST patterns. However, SST patterns and upwelling intensity during the Late Holocene are similar to present-day patterns, both in southern Peru and central-north Chile (Carré et al., 2012, 2014, 2016; Ortlieb et al., 2011; Vargas et al., 2006). These studies highlight important changes in paleoceanographic dynamics during the Holocene, yet they have been restricted to locations at the extremes of a vast region (e.g. >12° latitude) and have chronological hiatuses (but see Salvatteci et al., 2019a). Our study aims to contribute filling geographic and temporal gaps taking advantage of a near-continuous paleoceanographic record derived from shellfish carbonate from the keyhole limpet *Fissurella maxima* collected from archaeological stratigraphic sequences located in the Taltal area. The steep topography and bathymetry of our study region (Fig. 1) intensify alongshore upwelling-favorable winds and allow recently upwelled water to move onshore, respectively (Piñones et al., 2007). This work presents the first trans-Holocene record of nearshore $\delta^{18}O$-SST and $\delta^{13}C$ for the Pacific coast of South America, thus contributing to our understanding of nearshore paleoceanographic variability and variations in coastal ecosystem characteristics.

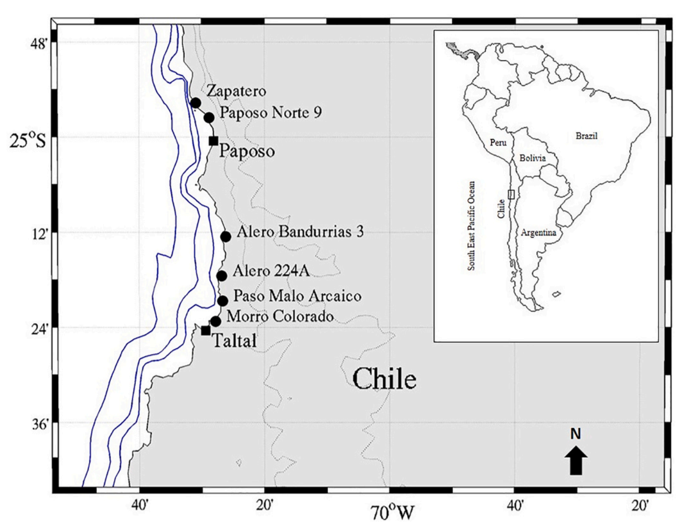


**Fig. 1.** Map of the study area, locations of the archaeological sites (bold circles) and fishing towns (bold squares) where *F. maxima* samples were collected for paleotemperature and modern temperature analyses, respectively. Dotted contours over land (gray area) indicate 1000 and 1500 masl, respectively, while the blue lines in the ocean denote the −500, −200, −100 m isobaths. Note the steep coastal platform and the narrow continental shelf along the study area. The inset on the upper right indicates the study location on the coast of western South America. (For interpretation of the references to colour in this figure legend, the reader is referred to the web version of this article.)

## 2. Materials and methods

Our study is based on carbonate data from 49 *F. maxima* shells. Their ecology and biology is presented in Flores et al. (2018). Eight modern shells were obtained locally during 2015–2016 around Paposo and Taltal, and 41 shells come from six archaeological shell midden deposits (Fig. 1 and Supplementary Table 1). All archaeological shells were radiocarbon dated in the Keck Carbon Cycle AMS Laboratory at the University of California Irvine and Northern Arizona University Amino Acid Geochronology Laboratory. All ages were calibrated using Calib 7.1 (Stuiver et al., 2020), SHCal 13 curve and corrected for reservoir effect following regional estimates from northern Chile (Ortlieb et al., 2011) (Supplementary Table 1). Shell sampling and processing for $\delta^{18}O$ and $\delta^{13}C$ isotopic analyses was carried out following methodology described in previous studies (Flores, 2017; Glassow et al., 2012; Jew et al., 2016), more specifically, replicating sampling strategy previously published by ourselves on modern and archaeological *F. maxima* shells (Flores et al., 2018). In brief, we took eight samples per shell along the growth axis obtaining approximately 0.3–0.5 mg of carbonate powder from each one. See Flores et al. (2018) for further details on sampling strategy and *F. maxima* shell as proxy for SST. A total of 384 shell carbonate samples were sent to the Stable Isotope Facility at the University of California, Davis (see Flores et al., 2018 for further details on sampling and *F. maxima* shell as proxy for SST). Oxygen and carbon isotopic composition were calibrated relative to the Vienna Pee Dee Belemnite (VPDB) scale using NBS-18 (−5.01‰ for $\delta^{13}C$ and − 23.01‰ for $\delta^{18}O$) and NBS-19 (−2.20‰ $\delta^{18}O$, 1.95‰ $\delta^{13}C$), and instrumental standard deviation was 0.1‰ for $\delta^{13}C$ and 0.2‰ for $\delta^{18}O$.

$\delta^{18}O$ values obtained from archaeological shells were corrected for ice volume effect on seawater $\delta^{18}O$ through the Holocene. Correction values were calculated using the global sea level reconstruction from Lambeck and Chappell (2001) and a maximum ice volume effect of 1.05‰ for the last glacial maximum (LGM) (Duplessy et al., 2002) (see corrected values in Supplementary Table 2). Correction values were obtained considering the known sea level at a specific time, divided by the lowest sea level recorded between the LGM and the point of major ice sheet decay (22,000 cal years to present time, Lambeck and Chappell, 2001). This value is then multiplied by the difference in seawater $\delta^{18}O$ values between the LGM and today (Duplessy et al., 2002) (correction value = (sea level at specific time/145)*1.05).

$\delta^{13}C$ values obtained from modern shells were corrected for the Suess effect to account for the $\delta^{13}C$ depleted CO2 emitted to the atmosphere by the anthropogenic combustion of fossil fuel (Bacastow et al., 1996; Keeling, 1979; Quay et al., 1992) (see values in Supplementary Table 2). The Suess effect correction was calculated by adding 0.5‰ to $\delta^{13}C$ values of modern shells (Eide et al., 2017a). Finally, to transform corrected $\delta^{18}O$ values from modern and archaeological shells to SST data, we used the equation of Ford et al. (2010), with mean $\delta^{18}O$ seawater value of −0.01‰ obtained from local measurements at the study area (Flores et al., 2018). Although Early Holocene SST values have been presented previously (Flores et al., 2018), none of the associated dates nor $\delta^{13}C$ values have been previously published.

## 3. Results

Dates obtained for each of the 41 archaeological shells, situate SST and $\delta^{13}C$ data along the entire Holocene with a gap between 9600 and 7600 cal yr BP (Supplementary Table 1, Fig. 2). Reconstructed SST time series (Fig. 2A) shows the coolest conditions during the Early Holocene (mean SST 13.0 °C to 15.7 °C, from 11,120 to 9680 cal yr BP, Supplementary Table 1), followed by the warmest temperatures at the beginning of the Middle Holocene (mean SST 16.3 °C to 17.7 °C, from 7630 to 6960 cal yr BP, Supplementary Table 1). A decrease in SST is observed during the rest of the Middle Holocene, with the coolest record between 4900 and 4300 cal yr BP (mean SST 13.6 °C to 15.4 °C, Supplementary Table 1). Finally, for the Late Holocene, we observed a variable trend towards warmer mean SST (mean SST 13.0 °C to 16.6 °C, from 2830 to 630 cal yr BP, Supplementary Table 1). Compared to archaeological times, reconstructed SST from modern shells are similar to the beginning of the Middle Holocene (mean SST 15.8 °C to 17.9 °C, Supplementary Table 1, Fig. 2B). Based on a previous study reporting a temperature offset between reconstructed SST from modern *F. maxima* shells and in situ SST (Flores et al., 2018), our SST records from archaeological and modern shells have to be considered with an approximate deviation of +1.0 °C from in situ SST.

$\delta^{13}$C values from *F. maxima* shells also change through time (Fig. 2C, Supplementary Table 1). Shells from the Early Holocene are generally the most $\delta^{13}$C-depleted of the sequence (mean values −0.61‰ to 0.97‰, Supplementary Table 1). A contrasting pattern is observed at the beginning of the Middle Holocene with exclusively enriched values (mean value 0.33‰ to 0.88‰, Supplementary Table 1). Along the Middle Holocene, a more variable record is observed with values distributed mostly above 0‰ (mean value −0.39‰ to 0.82‰, Supplementary Table 1). Finally, from around 3600 cal yr BP, the Late Holocene presents even higher variability than previously and a trend towards $\delta^{13}$C positive values (mean value −0.36‰ to 1.47‰, Supplementary Table 1). Compared to archaeological times, modern *F. maxima* $\delta^{13}$C corrected values show little variation among them and gather mostly below 0‰ (mean values ranging from −0.77‰ to 0.21‰, Supplementary Table 1, Fig. 2D). Modern $\delta^{13}$C values depart from the coupling with SST observed during the Holocene as they are uniformly $\delta^{13}$C-depleted, with only one shell showing a mean above zero. Fluctuations in $\delta^{13}$C are significantly related to changes in SST during the Holocene ($r^2 = 0.173$ $p = 0.006$, $F = 8.164$, dfe = 39). The relationship is not significant when modern shells are incorporated in the analysis.

## 4. Discussion

Our results, from 25°S, represent the first continuous record of nearshore paleoceanographic variability during the Holocene amid a vast section off western South America (18°- 31°S). To this end, they contribute to fill a gap in our understanding of the spatial structure of the SST field over this period and offer some insights into potential changes of coastal ecosystem characteristics.

Except for a temporal hiatus during the Early Holocene, which coincides with a lacuna in the archaeological record of the area (Salazar et al., 2015), our carbonate trans-Holocene record shows a consistent between SST and $\delta^{13}$C. Deep and older water brought to the surface by coastal upwelling is characterized by low temperature, high nutrient and low oxygen concentrations, following its origin in the oxygen minimum zone (OMZ) off the eastern tropical and subtropical Pacific (Strub et al., 1998; Chavez and Messié, 2009; Salvatteci et al., 2019a, 2019b). The water in the Ekman layer along the coast of southern Peru and northern Chile is a mixture of Subtropical and Equatorial Subsurface Water (Silva et al., 2009), and is $\delta^{13}$C depleted (Martínez-Méndez et al., 2013; Sadler et al., 2012). Previous studies have suggested that shell $\delta^{13}$C can reflect $\delta^{13}C_{DIC}$ incorporated from upwelled waters (Andrus et al., 2005; Carré et al., 2005; Gosselin et al., 2013; Sadler et al., 2012; Ferguson et al., 2013). Most of these studies, together with mechanistic attempts to link $\delta^{13}C_{DIC}$ to $\delta^{13}$C in the shells, have pointed out the complexity of this approach (McConnaughey and Gillikin, 2008). However, it is interesting to note regional differences in $\delta^{13}C_{DIC}$ in seawater between southern California and southern Peru, where $\delta^{13}C_{DIC}$ values in coastal seawater are more negative in the latter (Sadler et al., 2012; Ferguson et al., 2013). After correcting aragonite $\delta^{13}$C values from metabolic and kinetic effect for bivalve shells from southern Peru,

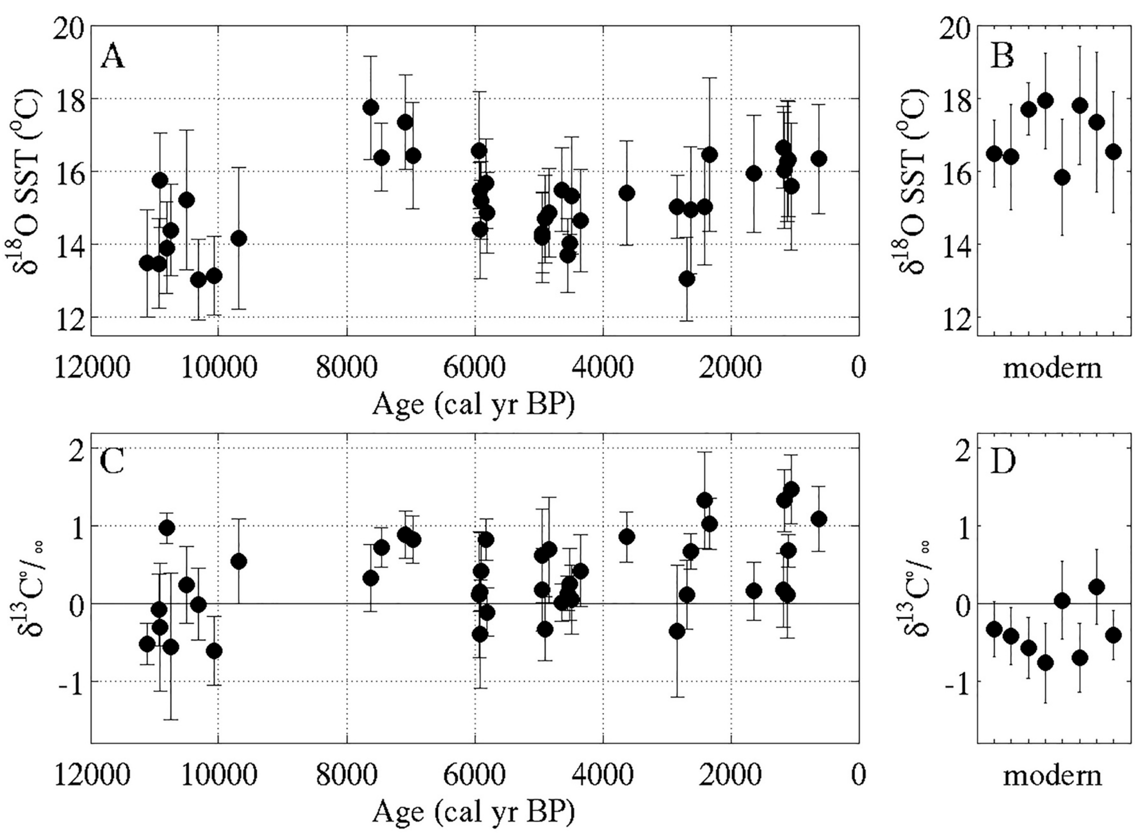


**Fig. 2.** Trans-Holocene record of A) past and B) present SST and C) past and D) present $\delta^{13}$C corrected values for the southern Coast of the Atacama Desert (25°S). Each solid dot and dashed bar indicates mean +/− 1 SD for eight carbonate samples for an individual *F. maxima* shell. The horizontal solid lines on C and D indicate equilibrium conditions between atmospheric and ocean-dissolved $\delta^{13}$C with negative values suggesting the presence of deeper, $\delta^{13}$C-depleted waters (e.g. Ferguson et al., 2013).

Ferguson et al. (2013) attributed their co-variation with $\delta^{18}O$ to changes in upwelling intensity during the Middle Holocene and present times. Following the temporal association shown by our data between increasing/decreasing mean values of $\delta^{13}C$ and cooler/warmer SST, and keeping in mind the caveats above, temporal variation $\delta^{13}C$ will be used as a proxy for nearshore oceanographic changes throughout the Holocene.

Our trans-Holocene record supports previous results showing cooler than present SST during the Early Holocene and intense upwelling-favorable conditions along the arid-hyperarid coast (18°-25°S) of western south America (Carré et al., 2014; Flores et al., 2018; Ortlieb et al., 2011; Vargas et al., 2006). During the same period, isotopic records from archaeological shell carbonate from the coast of central-north Chile (31°S), indicate warmer waters and weaker upwelling intensity (Carré et al., 2012, 2016). As discussed in previous studies, this latitudinal contrast may originate following a combination of factors, from varying upwelling intensity to a reorganization of water masses (Carré et al., 2016; Flores et al., 2018; Fontugne et al., 2004; Ortlieb et al., 2011). Although our data cannot discriminate water mass origin, the cooler waters detected around 25°S in the Early Holocene imply higher nutrient content, likely through enhanced coastal upwelling.

The warmest temperatures of our shell record, at the beginning of the Middle Holocene, were accompanied by enriched $\delta^{13}C$ values, which may follow from weakened coastal upwelling. Alkenone-derived SST records from sediment cores off southern Peru (17°S, Salvatteci et al., 2019a) suggest a cooling associated to intense upwelling conditions during the Middle Holocene (Sadler et al., 2012). A little bit south, other studies on marine sediment cores at 24°S (Mohtadi et al., 2004), 30°S (Kaiser et al., 2008), and 32°S (Kim et al., 2002) have reconstructed warmer than present SST offshore north central Chile. On the other hand, shell carbonate SST record at 18°S, depicts nearshore water temperatures as cold as the ones registered for Taltal during the Early Holocene (Carré et al., 2012). Cold inshore and offshore SST at 17–18°S may be interpreted as an oceanographic situation where the coastal transition zone is far from shore. On the other hand, the difference at 30–32°S between offshore and nearshore SST has been suggested as evidence of a seaward temperature gradient similar to present times (Carré et al., 2012, 2016). For the case of Taltal, albeit the small sample size supporting a warm event between 7600 and 6900 cal yr BP, our four samples show a coherent SST pattern among them (Fig. 2A), suggesting that warmer than present SST, inshore and offshore, at 24–25°S during this time may be linked to a weak seaward temperature gradient. Regarding radiocarbon reservoir ages for the Middle Holocene, they suggest intense upwelling conditions for southern Peru (18°S) and weak conditions for north central Chile (31°S) until around 6900 cal yr BP (Carré et al., 2016; Ortlieb et al., 2011). For the area of Taltal at 24–25°S, although there is no information on radiocarbon reservoir ages, our enriched $\delta^{13}C$ values obtained from limpet archaeological shells, together with a multiproxy sediment analysis done by Mohtadi et al. (2004), suggest weakened coastal upwelling conditions. Further coeval paleoceanographic data from north and south of Taltal will be necessary to evaluate whether oceanographic conditions at the beginning of the Mid-Holocene decouple from those observed in other areas. After the SST peak at the beginning of the Middle Holocene in the Taltal record, the rest of the period shows a decrease in SST until ~4300 cal yr BP, accompanied by relatively $\delta^{13}C$-depleted values. Our results indicate that between 6900 and 4300 cal yr BP, nearshore conditions of the Atacama desert experienced cool ocean temperatures, similar to those observed from southern Peru to central Chile (Carré et al., 2012; Kim et al., 2002; Sadler et al., 2012), likely associated to a weak OMZ (Salvatteci et al., 2016, 2019a).

The sustained warming during the rest of the Late Holocene until around 600 cal yr BP, is consistently related to enriched $\delta^{13}C$ values. This observation is well in line with evidence of weakened upwelling in southern Peru and northern-central Chile (Carré et al., 2016) supporting a region-wide weakening of coastal upwelling during this time period.

Finally, although modern SST values are among the highest of our record, $\delta^{13}C$ values are the most depleted of our study, even after the Suess effect correction (Fig. 2D). We hypothesize that this pattern is consistent with the extremely strong upwelling recorded over the current warm period (Salvatteci et al., 2019b) and compounded by the large ENSO event recorded during the time when we collected modern *F. maxima* shells (2015–2016, Flores et al., 2018; Santoso et al., 2017). High SST and depleted $\delta^{13}C$ values have been also identified in mollusk shells from Peru that recorded 1982–1983 El Niño event (Andrus et al., 2005).

Regarding possible ecological consequences of paleoceanographic reconstructions, conditions of cold/warm SST and intensified/weaken upwelling would have implied different general scenarios. Studies have shown that a strong OMZ is consistent with high productivity in the photic layer under upwelling conditions (Chavez and Messié, 2009; Salvatteci et al., 2019b). Subsequently, in benthic habitats, coastal upwelling sustains high abundance of *Laminarian* algae (i.e. kelp, Bell et al., 2018; Broitman et al., 2001), together with the diverse fish and shellfish assemblage that occupy these complex coastal environments (Pérez-Matus et al., 2017). At the same time, intense upwelling transports the planktonic larvae of benthic species offshore (Menge et al., 2003; Caley et al., 1996). Thus, the size of benthic adult populations is limited in areas where coastal upwelling is intensified, such as capes or headlands, whereas an opposite pattern is observed inside embayments where larvae are retained together with warmer waters (Largier, 2020). Worldwide, sharp spatial transitions in the abundance of different shellfish functional groups have been observed between areas either sheltered or exposed to coastal upwelling (Navarrete et al., 2005; Wieters et al., 2009; Largier, 2020). For pelagic habitats, multidecadal changes in the spatial structure of the OMZ have been shown to modify the distribution and regional patterns of abundance of coastal-pelagic fish species. For example, during periods of intense upwelling and strong OMZ, species such as Jack mackerel (*Trachurus murphyi*) and sardines (*Sardinops sagax*) are displaced offshore, whereas Anchovies (*Engraulis ringens*) seem to tolerate low oxygen conditions and remain closer to the coast (Bertrand et al., 2011, 2016). Consequently, the large temporal fluctuations in SST and coastal upwelling intensity observed across the Holocene in the northern coast of Chile, likely influenced the local abundance and spatial distribution of benthic invertebrates and coastal and pelagic fish species over time (Graham et al., 2009; Erlandson and Fitzpatrick, 2006). Archaeological data from the area show interesting changes in fish assemblages that may support our ecological interpretations. For example, Early Holocene sites are characterized by cold-tolerant fish species, and Middle Holocene sites show a sharp increase in the abundance of the coastal pelagic Jack mackerel and the presence of open–sea taxa (i.e. *Xiphias gladius, Kajikia audax*) previously absent in the zooarchaeological record (Béarez et al., 2016; Olguín et al., 2014; Rebolledo et al., 2016).

Fig. 1.Map of the study area, locations of the archaeological sites (bold circles) and fishing towns (bold squares) where *F. maxima* samples were collected for paleotemperature and modern temperature analyses, respectively. Dotted contours over land (gray area) indicate 1000 and 1500 masl, respectively, while the blue lines in the ocean denote the −500, −200, −100 m isobaths. Note the steep coastal platform and the narrow continental shelf along the study area. The inset on the upper right indicates the study location on the coast of western South America.

Fig. 2.Trans-Holocene record of A) past and B) present SST and C) past and D) present $\delta^{13}C$ corrected values for the southern Coast of the Atacama Desert (25°S). Each solid dot and dashed bar indicates mean +/− 1 SD for eight carbonate samples for an individual *F. maxima* shell. The horizontal solid lines on C and D indicate equilibrium conditions between atmospheric and ocean-dissolved $\delta^{13}C$ with negative values suggesting the presence of deeper, $\delta^{13}C$-depleted waters (e.g. Ferguson et al., 2013).

## 5. Conclusions

The present work is the first Trans-Holocene estimate of SST and $\delta^{13}C$ of the Eastern Pacific Coast based on archaeological marine shells. The congruence and differences between Taltal (25°S) and similar nearshore paleoceanographic data from Southern Peru (18°S) and central-north Chile (31°S), suggest complex changes in the oceanographic dynamics along the Pacific Coast of South America throughout the Holocene. In this way, during the Early Holocene, the latitudinal difference in SST and upwelling intensity showed an opposite pattern to modern times, with the coast between 18°- 25°S experiencing more intense upwelling than between 25°- 31°S. Then, between 7600 and 6900 cal yr BP, Taltal decoupled from regional records showing extremely warm waters that may be linked to mesoscale structure in nearshore oceanographic conditions observed along upwelling ecosystems worldwide (Wieters et al., 2009; Helmuth et al., 2006). Finally, oceanographic conditions seem to homogenize along the Peru-Chile coast from the Late Holocene until 600 cal yr BP, with a steady decrease in upwelling intensity and increase in SST.

The magnitude of paleoceanographic changes documented in our results provide strong support for major reorganizations of nearshore benthic and pelagic ecological communities in space and time, which likely impacted marine resource availability for ancient fishermen groups. Archaeological data on marine fauna from the study area seems to support our general observations but more information is necessary to evaluate the different scenarios. Further research at locations between 18°- 31°S is needed to explore changes in the structure of the Humboldt Current along the Holocene at a small spatial scales, and their influence on resources availability and human adaptation through the prehistory of South America.

Finally, the preindustrial SST and $\delta^{13}C$ values derived from archaeological shells of the Atacama Desert Coast, will represent an important contribution to the modeling of past global ocean circulations (Eide et al., 2017a, 2017b).

Supplementary data to this article can be found online at https://doi.org/10.1016/j.palaeo.2020.110090.

## Declaration of Competing Interest

None.

## Acknowledgments

This work was supported by the National Fund for Scientific and Technological Development (FONDECYT 3170913, 1181300, 1151203) and Millennium nucleus MUSELS and UPWELL funded through ICM. Special thanks to Marcelo Rivadeneira and Patricio Manríquez for their support during shell sample processing (lab space and sampling tools). Thanks to Laura Olguín and Javiera Guardia for helping gather shell samples, to Daniel Hernández for helping with shell processing, Pedro Andrade for shell dating calibration, and Diego Salazar and Matthieu Carré for supporting the overall research. Finally, we also want to acknowledge the anonymous reviewers for their sharp eye and suggestions on an earlier version of this manuscript.

## References

Aguilera, M.A., Aburto, J.A., Bravo, L., Broitman, B.R., García, R.A., Gaymer, C.F., Gelcich, S., López, B.A., Montecino, V., Pauchard, A., Ramos, M., Rutllant, J.A., Sáez, C.A., Valdivia, N., Thiel, M., 2019. Chapter 29. Chile: Environmental status and future. In: Sheppard, C. (Ed.), World Seas: An Environmental Evaluation. Volume I Europe, The Americas and West Africa. Academic Press.

Anderson, D., Maasch, K., Sandweiss, D., 2007. Climate Change and Cultural Dynamics. A global perspective on Mid-Holocene Transitions. Academic Press, London.

Andrus, C.F.T., Hodgins, G.W.L., Sandweiss, D.H., Crowe, D.E., 2005. Molluscan radiocarbon as a proxy for El Niño–related upwelling variation in Peru. In: Mora, G., Surge, D. (Eds.), Isotopic and Elemental Tracers of Cenozoic Climate Change, vol. 395. Geological Society of America Special Paper, pp. 13–20. https://doi.org/10.1130/SPE395.

Bacastow, R.B., Keeling, C.D., Lueker, T.J., Wahlen, M., Mook, W.G., 1996. The $^{13}C$ Suess effect in the world surface oceans and its implications for oceanic uptake of CO2: Analysis of observations at Bermuda. Glob. Biogeochem. Cycles 10, 335–346. https://doi.org/10.1029/96GB00192.

Béarez, P., Fuentes-Mucherl, F., Rebolledo, S., Salazar, D., Olguín, L., 2016. Billfish foraging along the Northern coast of Chile during the Middle Holocene (7400–5900 cal BP). J. Anthropol. Archaeol. 41, 185–195.

Bell, T.W., Reed, D.C., Nelson, N.B., Siegel, D.A., 2018. Regional patterns of physiological condition determine giant kelp net primary production dynamics. Limnol. Oceanogr. 63 (1), 472–483. https://doi.org/10.1002/lno.10753.

Bertrand, A., Chaigneau, A., Peraltilla, S., Ledesma, J., Graco, M., Monetti, F., Chavez, F. P., 2011. Oxygen: a fundamental property regulating pelagic ecosystem structure in the coastal southeastern tropical pacific. PLoS One 6 (12), e29558. https://doi.org/10.1371/journal.pone.0029558.

Bertrand, A., Habasque, J., Hattab, T., Hintzen, N.T., Oliveros-Ramos, R., Gutiérrez, M., Demarcq, H., Gerlotto, F., 2016. 3-D habitat suitability of jack mackerel Trachurus murphyi in the Southeastern Pacific, a comprehensive study. Prog. Oceanogr. 146, 199–211. https://doi.org/10.1016/j.pocean.2016.07.002.

Broitman, B.R., Navarrete, S.A., Smith, F., Gaines, S.D., 2001. Geographic variation of southeastern Pacific intertidal communities. Mar. Ecol. Prog. Ser. 224, 21–34. https://doi.org/10.3354/meps224021.

Caley, M.J., Carr, M.H., Hixon, M.A., Hughes, T.P., Menge, B.A., Jones, G.P., Menge, B. A., 1996. Recruitment and the local dynamics of open marine populations. Annu. Rev. Ecol. Evol. Syst. 27, 477–500. https://doi.org/10.1146/annurev.ecolsys.27.1.477.

Carré, M., Bentaleb, I., Fontugne, M., Lavallee, D., 2005. Strong El Niño events during the early Holocene: stable isotope evidence from Peruvian sea shells. The Holocene 15 (1), 42–47. https://doi.org/10.1191/0959683605h1782rp.

Carré, M., Azzoug, M., Bentaleb, I., Chase, B.M., Fontugne, M., Jackson, D., Ledru, M.P., Maldonado, A., Sachs, J.P., Schauer, A.J., 2012. Mid-Holocene mean climate in the south eastern Pacific and its influence on South America. Quat. Int. 253, 55–66. https://doi.org/10.1016/j.quaint.2011.02.004.

Carré, M., Sachs, J.P., Purca, S., Schauer, A.J., Braconnot, P., Falcón, R.A., Julien, M., Lavallée, D., 2014. Holocene history of ENSO variance and asymmetry in the eastern tropical Pacific. Science 345, 1045–1048. https://doi.org/10.1126/science.1252220.

Carré, M., Jackson, D., Maldonado, A., Chase, B.M., Sachs, J.P., 2016. Variability of $^{14}C$ reservoir age and air-sea flux of $CO^2$ in the Peru-Chile upwelling region during the past 12,000 years. Quat. Res. 85, 87–93. https://doi.org/10.1016/j.yqres.2015.12.002.

Caviedes, C., 2002. El Niño in History: Storming through the Ages. University Press Florida, Gainesville.

Chavez, F.P., Messié, M., 2009. A comparison of Eastern boundary upwelling ecosystems. Prog. Oceanogr. 83 (1–4), 80–96. https://doi.org/10.1016/j.pocean.2009.07.032.

Duplessy, J.C., Labeyrie, L., Waelbroeck, C., 2002. Constraints on the ocean oxygen isotopic enrichment between the last glacial maximum and the holocene: paleoceanographic implications. Quat. Sci. Rev. 21, 315–330. https://doi.org/10.1016/S0277-3791(01)00107-X.

Eide, M., Olsen, A., Ninnemann, U.S., Eldevik, T., 2017a. A global estimate of the full oceanic 13C Suess effect since the preindustrial. Glob. Biogeochem. Cycles 31, 492–514. https://doi.org/10.1002/2016GB005472.

Eide, M., Olsen, A., Ninnemann, U.S., Johannessen, T., 2017b. A global ocean climatology of preindustrial and modern ocean δ 13C. Glob. Biogeochem. Cycles 31, 515–534. https://doi.org/10.1002/2016GB005473.

Erlandson, J.M., Fitzpatrick, S.M., 2006. Oceans, islands, and coasts: current perspectives on the role of the Sea in human prehistory. J. Island Coast. Archaeol. 1 (1), 5–32. https://doi.org/10.1080/15564890600639504.

Ferguson, J.E., Johnson, K.R., Santos, G., Meyer, L., Tripati, A., 2013. Investigating $\delta^{13}C$ and Δ14C within Mytilus californianus shells as proxies of upwelling intensity. Geochem. Geophys. Geosyst. 14 (6), 1856–1865. https://doi.org/10.1002/ggge.20090.

Flores, C., 2017. Importance of small-scale paleo-oceanographic conditions to interpret changes in size of California mussel (Mytilus californianus). Late Holocene, Santa Cruz island, California. Quat. Int. 427, 137–150. https://doi.org/10.1016/j.quaint.2016.01.036.

Flores, C., Gayo, E.M., Salazar, D., Broitman, B.R., 2018. $\delta^{18}O$ of Fissurella maxima as a proxy for reconstructing Early Holocene sea surface temperatures in the coastal Atacama desert (25°S). Palaeogeogr. Palaeoclimatol. Palaeoecol. 499, 22–34. https://doi.org/10.1016/j.palaeo.2018.03.031.

Fontugne, M., Carré, M., Bentaleb, I., Julien, M., Lavallée, D., 2004. Radiocarbon reservoir age variations in the South Peruvian upwelling during the Holocene. Radiocarbon. 46, 531–537. https://doi.org/10.1017/S003382220003558X.

Ford, H.L., Schellenberg, S.A., Becker, B.J., Deutschman, D.L., Dyck, K.A., Koch, P.L., 2010. Evaluating the skeletal chemistry of Mytilus californianus as a temperature proxy: effects of microenvironment and ontogeny. Paleoceanography 25 (1), PA1203. https://doi.org/10.1029/2008PA001677.

Glassow, M., Thakar, H.B., Kennett, D.J., 2012. Red abalone collecting and marine water temperature during the Middle Holocene occupation of Santa Cruz Island, California. J. Archaeol. Sci. 39, 2574–2582. https://doi.org/10.1016/j.jas.2012.03.017.

Gosselin, M., Lazareth, C.E., Ortlieb, L., 2013. Sclerochronological studies in the Humboldt current system, a highly variable ecosystem. J. Shellfish Res. 32 (3), 867–882. https://doi.org/10.2983/035.032.0331.

Graham, M.H., Kinlan, B.P., Grosberg, R.K., 2009. Post-glacial redistribution and shifts in productivity of giant kelp forests. Proc. R. Soc. B 277, 399–406. https://doi.org/10.1098/rspb.2009.1664.

Helmuth, B., Broitman, B.R., Blanchette, C.A., Gilman, S., Halpin, P., Harley, C.D.G., O'Donnell, M.J., Hofmann, G.E., Menge, B., Strickland, D., 2006. Mosaic patterns of thermal stress in the rocky intertidal zone: implications for climate change. Ecol. Monogr. 76, 461–479. https://doi.org/10.1890/0012-9615(2006)076[0461,MPOTSI]2.0.CO;2.

Hormazabal, S, Shaffer, G, Leth, O, 2004. Coastal transition zone off Chile. J. Geophys. Res. 109 (C1), C01021. https://doi.org/10.1029/2003JC001956.

Jew, N.P., Fitzpatrick, S.M., Sullivan, K.J., 2016. $\delta^{18}O$ analysis of Donax denticulatus: evaluating a proxy for sea surface temperature and nearshore paleoenvironmental reconstructions for the northern Caribbean. J. Archaeol. Sci. Rep. 8, 216–223. https://doi.org/10.1016/j.jasrep.2016.06.018.

Kaiser, J., Schefuß, E., Lamy, F., Mohtadi, M., Hebbeln, D., 2008. Glacial to Holocene changes in sea surface temperature and coastal vegetation in north Central Chile: high versus low latitude forcing. Quat. Sci. Rev. 21, 2085–2097.

Keeling, C.D., 1979. The Suess effect: $^{13}$Carbon-$^{14}$Carbon interrelations. Environ. Int. 2, 229–300. https://doi.org/10.1016/0160-4120(79)90005-9.

Kim, J.H., Schneider, R.R., Hebbeln, D., Muller, P.J., Wefer, G., 2002. Last deglacial sea-surface temperature evolution in the Southeast Pacific compared to climate changes on the South American continent. Quat. Sci. Rev. 21, 2085–2097 doi:Pii S0277-3791(02)00012-4\rDoi. https://doi.org/10.1016/S0277-3791(02)00012-4.

Lambeck, K., Chappell, J., 2001. Sea level change through the Last Glacial Cycle. Science 292 (5517), 679–686. https://doi.org/10.1126/science.1059549.

Largier, J.L., 2020. Upwelling bays: how coastal upwelling controls circulation, habitat, and productivity in bays. Annu. Rev. Mar. Sci. 12, 415–447. https://doi.org/10.1146/annurev-marine-010419-011020.

Martínez-Méndez, G., Hebbeln, D., Mohtadi, M., Lamy, F., De Pol-Holz, R., Reyes-Macaya, D., Freudenthal, T., 2013. Changes in the advection of Antarctic Intermediate Water to the northern Chilean coast during the last 970 kyr. Paleoceanography 28, 607–618. https://doi.org/10.1002/palo.20047.

Mayewski, P.A., Rohling, E.E., Stager, J.C., Karlén, W., Maasch, K.A., Meeker, L.D., Meyerson, E.A., Gasse, F., van Kreveld, S., Holmgren, K., Lee-Thorp, J., Rosqvist, G., Rack, F., Staubwasser, M., Schneider, R.R., Steig, E.J., 2004. Holocene climate variability. Quat. Res. 62 (3), 243–255. https://doi.org/10.1016/j.yqres.2004.07.001.

McConnaughey, T.A., Gillikin, D.P., 2008. Carbon isotopes in mollusk shell carbonates. Geo-Mar Lett. 28, 287–299. https://doi.org/10.1007/s00367-008-0116-4.

McMichael, A.J., 2012. Insights from past millennia into climatic impacts on human health and survival. Proc. Natl. Acad. Sci. U. S. A. 109 (13), 4730–4737.

Menge, B.A., Lubchenco, J., Bracken, M.E.S., Chan, F., Foley, M.M., Freidenburg, T.L., Webster, M.S., 2003. Coastal oceanography sets the pace of rocky intertidal community dynamics. Proc. Natl. Acad. Sci. U. S. A. 100 (21), 12229–12234. https://doi.org/10.1073/pnas.1534875100.

Mohtadi, M., Romero, O.E., Hebbeln, D., 2004. Changing marine productivity off Northern Chile during the past 19 000 years: a multivariable approach. J. Quat. Sci. 19, 347–360.

Montecino, V., Lange, C.B., 2009. The Humboldt current system: ecosystem components and processes, fisheries, and sediment studies. Prog. Oceanogr. 83 (1–4), 65–79.

Navarrete, S.A., Wieters, E.A., Broitman, B.R., Castilla, J.C., 2005. Scales of benthic-pelagic coupling and the intensity of species interactions: from recruitment limitation to top-down control. Proc. Natl. Acad. Sci. U. S. A. 102 (50), 18046–18051. https://doi.org/10.1073/pnas.0509119102.

Olguín, L., Salazar, D., Jackson, D., 2014. Tempranas Evidencias de Navegación y Caza de Especies Oceánicas en la Costa Pacífica de Sudamérica (Taltal, ~7.000 años cal. A.P.) Chungara, 46, pp. 177–192.

Ortlieb, L., Vargas, G., Saliège, J.F., 2011. Marine radiocarbon reservoir effect along the northern Chile-southern Peru coast (14-24°S) throughout the Holocene. Quat. Res. 75, 91–103. https://doi.org/10.1016/j.yqres.2010.07.018.

Pérez-Matus, A., Carrasco, S.A., Gelcich, S., Fernandez, M., Wieters, E.A., 2017. Exploring the effects of fishing pressure and upwelling intensity over subtidal kelp forest communities in Central Chile. Ecosphere 8 (5), e01808. https://doi.org/10.1002/ecs2.1808.

Piñones, A., Castilla, J.C., Guiñez, R., Largier, J., 2007. Nearshore surface temperatures in Antofagasta Bay (Chile) and adjacent upwelling centers. Ciencias Marinas 33 (1), 37–48. https://doi.org/10.7773/cm.v33i1.1226.

Quay, P.B., Tilbrook, B., Wong, C.S., 1992. Oceanic uptake of fossil fuel CO2: Carbon-13 evidence. Science 256, 74–79. https://doi.org/10.1126/science.256.5053.74.

Rebolledo, S., Béarez, P., Salazar, D., Fuentes, F., 2016. Maritime fishing during the Middle Holocene in the hyperarid coast of the Atacama Desert. Quat. Int. 391, 3–11.

Richardson, J., Sandweiss, D., 2008. Climate Change, El Niño, and the rise of complex society on the Peruvian coast during the Middle Holocene. In: Sandweiss, D., Quilter, J. (Eds.), El Niño. Catastrophism, and Culture Change in Ancient America. Harvard University Press, Washington, pp. 59–76.

Sadler, J., Carré, M., Azzoug, M., Schauer, A.J., Ledesma, J., Cardenas, F., Chase, B.M., Bentaleb, I., Muller, S.D., Mandeng, M., Rohling, E.J., Sachs, J.P., 2012. Reconstructing past upwelling intensity and the seasonal dynamics of primary productivity along the Peruvian coastline from mollusk shell stable isotopes. Geochem. Geophys. Geosyst. 13, Q01015 https://doi.org/10.1029/2011GC003595.

Salazar, D., Figueroa, V., Andrade, P., Salinas, H., Power, X., Rebolledo, S., Parra, S., Orellana, H., Urrea, J., 2015. Cronología y organización económica de las poblaciones arcaicas de la costa de Taltal. Estudios Atacameños 50, 7–46.

Salvatteci, R., Gutierrez, D., Sifeddine, A., Ortlieb, L., Druffel, E., Boussafir, M., Schneider, R., 2016. Centennial to millennial-scale changes in oxygenation and productivity in the Eastern Tropical South Pacific during the last 25,000 years. Quat. Sci. Rev. 131, 102–117. https://doi.org/10.1016/j.quascirev.2015.10.044.

Salvatteci, R., Schneider, R.R., Blanz, T., Mollier-Vogel, E., 2019a. Deglacial to holocene ocean temperatures in the Humboldt current system as indicated by alkenone paleothermometry. Geophys. Res. Lett. 46 (1), 281–292. https://doi.org/10.1029/2018GL080634.

Salvatteci, R., Gutierrez, D., Field, D., Sifeddine, A., Ortlieb, L., Caquineau, S., Baumgartner, T., Ferreira, V., Bertrand, A., 2019b. Fish debris in sediments from the last 25 kyr in the Humboldt current reveal the role of productivity and oxygen on small pelagic fishes. Prog. Oceanogr. 176, 102114. https://doi.org/10.1016/j.pocean.2019.05.006.

Santoso, A., Mcphaden, M.J., Cai, W., 2017. The defining characteristics of ENSO extremes and the strong 2015/2016 El Niño. Rev. Geophys. 55, 1079–1129. https://doi.org/10.1002/2017RG000560.

Silva, N., Rojas, N., Fedele, A., 2009. Water masses in the Humboldt current system: properties, distribution, and the nitrate deficit as a chemical water mass tracer for equatorial subsurface Water off Chile. Deep-Sea Res. II Top. Stud. Oceanogr. 56 (16), 1004–1020. https://doi.org/10.1016/j.dsr2.2008.12.013.

Strub, P.T., Mesías, J., Montecino, V., Rutlant, J., Salinas, S., 1998. Coastal Ocean circulation off western South America, Coastal Segment (6, E). In: Robinson, A.R., Brink, K.H. (Eds.), The Sea, vol. 11. Wiley, Hoboken, NJ, pp. 273–314.

Stuiver, M., Reimer, P.J., Reimer, R.W., 2020. CALIB 7.1 [WWW program] at. http://calib.org (accessed 2020-3-26).

Vargas, G., Rutllant, J., Ortlieb, L., 2006. ENSO tropical-extratropical climate teleconnections and mechanisms for Holocene debris flows along the hyperarid coast of western South America (17°-24°S). Earth Planet. Sci. Lett. 249, 467–483. https://doi.org/10.1016/j.epsl.2006.07.022.

Wieters, E.A., Broitman, B.R., Branch, G.M., 2009. Benthic community structure and spatiotemporal thermal regimes in two upwelling ecosystems: comparisons between South Africa and Chile. Limnol. Oceanogr. 54 (4), 1060–1072. https://doi.org/10.4319/lo.2009.54.4.1060.

Zhang, D.D., Lee, H.F., Wang, C., Li, B., Pei, Q., Zhang, J., An, Y., 2011. The causality analysis of climate change and large-scale human crisis. Proc. Natl. Acad. Sci. 108 (42), 17296–17301. https://doi.org/10.1073/pnas.1104268108.